K.A. BUGAEV,[1] A.I. IVANYTSKYI,[1] D.R. OLIINYCHENKO,[1,2] E.G. NIKONOV,[3] V.V. SAGUN,[1] G.M. ZINOVJEV[1]

[1] Bogolyubov Institute for Theoretical Physics, Nat. Acad. of Sci. of Ukraine
(14b, Metrolohichna Str., Kyiv 03680, Ukraine; e-mail: bugaev@th.physik.uni-frankfurt.de, a_iv_@ukr.net, dimafopf@gmail.com, v_sagun@ukr.net)

[2] FIAS, Goethe-University
(1, Ruth-Moufang Str., 60438 Frankfurt upon Main, Germany)

[3] Laboratory for Information Technologies, JINR
(Dubna 141980, Russia; e-mail: e.nikonov@jinr.ru)

NON-SMOOTH CHEMICAL FREEZE-OUT AND APPARENT WIDTH OF WIDE RESONANCES AND QUARK GLUON BAGS IN A THERMAL ENVIRONMENT

PACS 25.75.-q, 25.75.Nq

We develop a hadron resonance gas model with the Gaussian width of hadron resonances. This model allows us to treat the usual hadrons and the quark gluon bags on the same footing and to study the stability of the results obtained within different formulations of the hadron resonance gas model. We perform a successful fit of 111 independent hadronic multiplicity ratios measured in nuclear collisions at the center-of-mass energies $\sqrt{s_{NN}}$ = 2.7–200 GeV. We demonstrate also that, in a narrow range of the collision energy $\sqrt{s_{NN}}$ = 4.3–4.9 GeV, there exist the peculiar irregularities in various thermodynamic quantities found at the chemical freeze-out. The most remarkable irregularity is an unprecedented jump of the number of effective degrees of freedom observed in this narrow energy range, which is seen in all realistic versions of the hadron resonance gas model, including the model with the Breit–Wigner parametrization of the resonance width and the one with a zero width of all resonances. Therefore, the developed concept is called the non-smooth chemical freeze-out. We are arguing that these irregularities evidence the possible formation of quark gluon bags. In order to develop other possible signals of their formation, we study the apparent width of wide hadronic resonances and quark gluon bags in a thermal environment. Two new effects generated for the wide resonances and the quark gluon bags by a thermal medium are discussed here: the near-threshold thermal resonance enhancement and the near-threshold thermal resonance sharpening. These effects are also analyzed for the Breit–Wigner width parametrization. It is shown that, if the resonance decay thresholds are located far away from the peak of the resonance mass attenuation, then such a width parametrization leads to a stronger enhancement of the resonance pressure, as compared with the Gaussian one. On the basis of the new effects, we argue that the most optimistic chance to find experimentally the quark gluon bags may be related to their sharpening and enhancement in a thermal medium. In this case, the wide quark gluon bags can appear directly or in decays as narrow resonances that are absent in the tables of elementary particles and have the apparent width about 50–120 MeV and the mass about or above 2.5 GeV.

K e y w o r d s: chemical freeze-out, wide resonance enhancement, width sharpening.

1. Introduction

Last year, the MIT Bag model [1] celebrated its forty years anniversary. A physical picture about the color degrees of freedom confined inside some volume turned out to be very productive, and it is used as a corner stone in many subsequent phenomenological models developed in high-energy nuclear physics. In particular, the hadron bags model [2] very efficiently exploited this idea and, as compared with the statistical bootstrap model [3–5], opened entirely new possibilities to study the strongly interacting matter thermodynamics. Since the time moment of the hadron bags model formulation [2], its original framework was greatly extended, and we now have a variety of exactly solvable statistical models, which describe the deconfinement phase transition and a crossover. For instance, the quark gluon bag with surface tension model (QGBSTM) is able to describe the tricritical [6–9] and critical endpoints [10, 11], by using the mechanism which is typical of ordinary liquids. In Ref. [12], the authors studied the influence of an interplay between the color-flavor correlations and the definite volume fluctuations of large quark gluon (QG) bags on the order of the deconfinement phase transition and the critical endpoint properties (they considered the phase transitions of higher orders), while the previous analysis is extended in Ref. [13] to study the role of the chiral symmetry restoration although at the vanishing baryonic density. Work [14] is devoted to a thorough analysis of different internal symmetries of large QG bags and to an investigation of the chiral symmetry restoration effect on the QCD phase diagram properties at non-vanishing baryonic densities although at the expense of neglecting the realistic short-range repulsion between the constituents. In Ref. [15], the novel, but rather complicated way to account for the hard-core repulsion between the QG bags is thoroughly analyzed.

The most coherent statistical picture of quark gluon bags is, however, based on the finite width model (FWM) [16, 17]. The FWM allows one to consider these bags as heavy wide hadronic resonances. It involves not only the asymptotic spectrum of the quark gluon bags, but it also incorporates their finite and medium-dependent widths. The FWM naturally explains the absence of heavy hadronic resonances in the experimental mass spectrum compared to the Hagedorn mass spectrum [3]. The FWM explains also that, besides the large width, the QG bags are strongly suppressed (by about fifteen to sixteen orders of magnitude compared to light hadrons!) for temperatures below about a half of the Hagedorn temperature $T_{\rm H}$, i.e., for $T < \frac{1}{2}T_{\rm H}$, by the *subthreshold suppression*. The latter is a manifestation of the color confinement in terms of the FWM. This property of QG bags combined with their large width and a very large number of decay channels leads to great difficulties in their experimental identification (see a discussion in [18]).

Nevertheless, the experimental searches for QG bags within the existing programs and the planned ones stimulate a strong interest in the formulation of possible QG bag formation signals. However, the two key questions, namely where (at which energies) and how can one observe the QG bag formation, did not get the definite answers during these four decades passed since the MIT Bag model formulation. At the same time, the discrete part of the hadronic mass spectrum became a precise tool to extract the thermodynamic quantities at the moment of a chemical freeze-out (FO) (see the works of advanced followers [6–15] of the MIT Bag model, which is known as the hadron resonance gas model (HRGM) [19–25]). The chemical FO is the moment, at which the inelastic collisions cease to exist simultaneously for all sorts of particles. The recent improvements of the HRGM achieved in [21–25] allow one to successfully describe all particle yield ratios measured in the nuclear collisions at the center-of-mass energies from $\sqrt{s_{NN}} =$ 2.7 GeV to $\sqrt{s_{NN}} = = 2.76$ TeV. Therefore here, we develop a new formulation of the HRGM, which involves the Gaussian mass attenuation of hadronic resonances instead of the Breit–Wigner one used in the previous versions of the HRGM. Such a model allows us to treat the usual hadrons and the QG bags of the FWM [16,17,27] on the same footing and to study the stability of the results obtained within different formulations of the HRGM. Moreover, a thorough analysis of the HRGM performed here allows us to answer the two key questions formulated above.

In particular, we demonstrate that, in a narrow range of collision energies $\sqrt{s_{NN}} = 4.3$–4.9 GeV, there exist the peculiar irregularities in various thermodynamic quantities calculated at the chemical FO. The most remarkable irregularity is an unprecedented jump of the number of effective degrees of freedom measured in the ratios $s^{\rm FO}/(T^{\rm FO})^3$ (it jumps by 1.67 times) and $p^{\rm FO}/(T^{\rm FO})^4$ (it jumps by 1.5 times), where

$s^{\rm FO}$, $T^{\rm FO}$, and $p^{\rm FO}$ denote the entropy density, the temperature, and the pressure taken, respectively, at the chemical FO. In order to distinguish the present chemical FO concept from the other ones, we name it *the non-smooth chemical FO*. On the basis of the FWM, we argue that these irregularities, which are observed in all versions of the HRGM analyzed here, are, possibly, related to the formation of QG bags.

In order to answer the second key question, we study a modification of the wide resonances in a thermal environment and perform a similar analysis for the QG bags. Our analysis shows that, even at the chemical FO, a thermal environment modifies essentially the resonance mass distribution in case of large widths, by leading to their narrowing and enhancement near the threshold. Based on these findings, we are arguing that the QG bags may be observed in the energy range $\sqrt{s_{NN}} \simeq 4.9$–6 GeV as the narrow resonances having the width of about 50–120 MeV and the mass about or above 2.5 GeV, which are absent in the tables of elementary particle properties.

The work is organized as follows. The next section describes the basic equations of the suggested HRGM. In Section 3, we present and discuss the particle yield ratios measured at the collision energies $\sqrt{s_{NN}} = 2.7$–200 GeV. The main attention is devoted to a discussion of the found irregularities. In Section 4, the apparent widths of wide resonances and QG bags are thoroughly analyzed. Our conclusions and some perspectives are discussed in Section 5.

2. Hadron Resonance Gas Model with Gaussian Mass Attenuation

As a discrete part of the hadron mass-volume spectrum, the HRGM [19–25] is contained in all elaborated statistical models of strongly interacting matter discussed above. In fact, it is a truncated hadronic mass spectrum of the statistical bootstrap model [3–5], which, however, accounts for the hard-core repulsion of hadrons and their width. The HRGM treats all hadron resonances known from the tables of particle properties [26] with masses up to $M_0 \simeq 2.5$ GeV as the interacting gas of Boltzmann particles. Its basic equations define the pressure $p(T, \{\mu\})$ of such a system with its temperature T and the set of chemical potentials $\{\mu\}$

$$p(T, \{\mu\}) \equiv T \sum_k F_k(\sigma_k) \exp\left[\frac{\mu_k - b_k p}{T}\right], \qquad (1)$$

$$F_k(\sigma_k) \equiv g_k \int\limits_0^\infty dm\, \frac{\Theta\left(m - M_k^{\rm Th}\right)}{N_k(M_k^{\rm Th})} \times$$

$$\times \exp\left[-\frac{(m_k - m)^2}{2\,\sigma_k^2}\right] \phi(m, T), \qquad (2)$$

$$\phi(m, T) \equiv \int \frac{d^3p}{(2\pi)^3} \exp\left[-\frac{\sqrt{p^2 + m^2}}{T}\right]. \qquad (3)$$

In Eq. (1), the sum runs over all hadrons and includes the following parameters for each k-th particle: the full chemical potential of the k-th hadron sort $\mu_k \equiv Q_k^B \mu_B + Q_k^S \mu_S + Q_k^{I3} \mu_{I3}$ is expressed in terms of the corresponding charges Q_k^L (Q_k^B is its baryonic charge, Q_k^S is its strange charge, and Q_k^{I3} is its third isospin projection charge) and their chemical potentials, m_k is its mean mass, g_k is its degeneracy factor, b_k is its excluded volume, while σ_k is the Gaussian width of this resonance which defines the true resonance width as $\Gamma_k = Q\,\sigma_k$ (with $Q \equiv 2\sqrt{2\,\ln 2}$), and the normalization factor is defined via the threshold mass $M_k^{\rm Th}$ of the dominant channel as

$$N_\sigma(M_k^{\rm Th}) \equiv \int\limits_{M_k^{\rm Th}}^\infty dm\ \exp\left[-\frac{(m_k - m)^2}{2\,\sigma^2}\right]. \qquad (4)$$

The hard core repulsion of the van der Waals type generates the suppression factor $\exp(-b_k\,p/T)$. The quantity $\phi(m, T)$ denotes the thermal particle density per spin-isospin degree of freedom of the hadron sort of mass m.

Note that a new important feature of the present HRGM formulation is the inclusion of the Gaussian width for all hadronic resonances. Such a feature allows us to treat the usual hadrons and the QG bags of the FWM, which must necessarily have the Gaussian width [16, 17, 27] on the same footing. This is a generalization of the most successful formulation of the HRGM [20–23], in which the hadronic excluded volumes $\{b_k\}$ are usually chosen to be equal, i.e., $b_1 = b_2 = ... = b_n \equiv b$. Note that the hadron resonance gas model [20, 22, 23] with the excluded volume $b = \frac{16}{3}\pi R^3 \simeq 0.45$ fm^3 and the hard-core radius $R = 0.3$ fm is able to successfully describe the ratios of hadronic multiplicities measured at the midrapidity in nuclear collisions for the center-of-mass energies from $\sqrt{s_{NN}} = 2.7$ GeV to $\sqrt{s_{NN}} = 2.76$ TeV. The main difference of the discrete mass-volume spectrum

of the present model from the one of the most popular version of the HRGM [20–23] is the usage of the Gaussian width in (3) instead of the Breit–Wigner one, although the effect is claimed to be below 10% even for wide hadronic resonances [20]. This feature of the present model is similar to the FWM of QG bags, where the presence of the Gaussian attenuation is of principal importance. It is so because the Breit–Wigner attenuation leads to a divergence of the FWM partition function [16, 17].

Despite its simplicity, the HRGM outlined above accurately accounts for the complexity of the strong interaction between hadrons. Indeed, the attraction between them is taken into account like in the statistical bootstrap model [3–5] via many sorts of hadrons, while the short-range interaction is modeled via the hard core repulsion, which leads to the appearance of the corresponding exponentials $\exp(-b_k\, p/T)$ in the spectrum (1). In principle, a surface tension induced by an interhadron interaction, like the one discussed recently in [28], should be considered for the mass-volume spectrum of hadrons used in (1). But the recent estimates made within the hadron resonance gas model [22] show that it is small. Hence, it is neglected here.

It is necessary to stress that the mass attenuation in Eqs. (1) and (2) has a clear physical meaning, and it is in line with the basic assumption of the statistical bootstrap model [3–5], which suggests to account for all hadronic states with their degeneracy, which can depend on the hadron mass. Therefore, the Gaussian or Breit–Wigner mass attenuation of hadronic resonances used in the HRGM accounts for the different hadronic states that belong to the same mass interval. This is evident, if one changes the order of a hadron sort summation and the mass integration in (1)

$$\frac{p(T,\{\mu\})}{T} \equiv \sum_k F_k(\sigma_k) \exp\left[\frac{\mu_k - b\, p}{T}\right] \equiv$$
$$\equiv \int\limits_0^\infty dm \sum_k \frac{\Theta\left(m - M_k^{\rm Th}\right)}{N_k(M_k^{\rm Th})} \exp\left[-\frac{(m_k - m)^2}{2\,\sigma_k^2}\right] \times$$
$$\times\, g_k\, \phi(m,T) \exp\left[\frac{\mu_k - b\, p}{T}\right]. \qquad (5)$$

Before analyzing the hadronic mass spectrum in a thermal environment, it is necessary to recall that the question of whether the experimental mass spectrum of hadrons given in the Particle Data Group tables coincides with the spectrum suggested by R. Hagedorn is of great interest nowadays [29–31]. However, almost all discussions of the hadron mass spectrum simply ignore the width of resonances, whereas it was found long ago that the large resonance width may essentially modify the spectrum [16–18, 32–37]. Therefore, it is important to study the effective mass spectrum of hadrons having a physical width. Another significant reason to introduce the width and decay channels of hadronic resonances into the HRGM is that, without accounting for the decays of wide resonances, it is impossible to accurately describe the particle yield ratios [20, 22]. For instance, the absence of the wide $\sigma(600)$-meson, which decays into two pions, does not allow one to correctly describe the pion yield, since just this meson alone is responsible for about 5 % of pions in the low AGS energy range. Therefore, the total particle density of hadrons of sort k consists of the thermal part $n_k^{\rm Th}$ and the decay one:

$$n_k^{\rm tot} \;=\; n_k^{\rm Th} + n_k^{\rm decay} = n_k^{\rm Th} + \sum_l n_l^{\rm Th}\, Br(l \to k), \qquad (6)$$

$$n_k^{\rm Th} \;\equiv\; \frac{\partial p}{\partial \mu_k} = \frac{F_k(\sigma_k) \exp\left[\frac{\mu_k - b\, p}{T}\right]}{1 + b \sum_l F_l(\sigma_l) \exp\left[\frac{\mu_l - b\, p}{T}\right]}, \qquad (7)$$

where $Br(l \to k)$ is the decay branching ratio of a hadron of the l-th sort into a hadron of the sort k. The masses, widths, and strong decay branchings of all hadrons are taken from the particle tables used by the thermodynamic code THERMUS [38].

The usage of a resonance mass attenuation of the Breit–Wigner (or Gaussian) type with the vacuum values of resonance masses and widths was heavily criticized in [39], but we find such a critique absolutely inadequate for the states below the chemical FO. First of all, we note that, in the approach of [39] and similar effective field theoretical models, the effect of a medium cannot be switched-off at any finite particle density or temperature. This means that, according to the treatment in [39] and [40] (and many similar works!), all the hadrons, whose momentum spectra are frozen due to the absence of any strong interaction between them, should keep their momentum-dependent widths and masses, which they acquired at the moment of kinetic FO up to their capture by detectors. Hence, according to

[39], all hadrons measured by detectors, including the stable ones, are some resonances that "feel" a thermal medium, in which they were produced long after the medium is gone. The typical examples of resonance mass attenuations obtained within the effective field theoretical models are shown in Fig. 1.

This problem is well-known in the transport simulations [41, 42]. Because the traditional field theoretical prescription does not provide the correct asymptotic solutions for the particles, which are stable in a vacuum, it was suggested to introduce the density-dependent coupling [42], which shifts the particles to their mass shell when they propagate to vacuum. Since there is no first-principle prescription for such a procedure, we conclude that the usage of the "crude" approximation (in terms of Ref. [39]) of Eq. (2) or the Breit–Wigner one is not only possible, but it is physically adequate after the chemical FO, when the inelastic reactions, except for the decays, cease to exist.

Second, all the "effects," which the authors of [39] claim to be of principal physical importance, are reduced to a slight (by about 20 MeV) shift of the mass attenuation peak and a small change in its shape for the Δ_{33} resonance, as one can see from Fig. 1. In our opinion, such modifications of the mass attenuation of the Δ_{33} resonance compared to the "crude" approximation of Eq. (2) cannot be measured in heavy ion experiments even for such narrow resonance as Δ_{33}, since its width in vacuum is known with the accuracy of a couple of MeVs [26]. Therefore, a serious discussion of similar "effects" for heavy hadronic resonances, whose masses and widths are often known with an accuracy of 100 MeV or 200 MeV (or worse) [26], does not make any sense. Thus, at the present state of art, there is no alternative to the physically transparent equation (2) to be used at and after the moment of the chemical FO. Below, it will be shown that the finite temperature affects the resulting mass distributions of resonances much more than those tiny modifications discussed in [39]. Moreover, none of the existing field theoretical models is able to tell us which a mass attenuation can be used for the QG bags (for a fresh critique of the standard field theoretical approach, see [43]), whereas the requirement of internal consistency of the FWM [16, 17] leads to the Gaussian mass attenuation for the QG bags or the heavy and wide resonances. Furthermore, the FWM allows one to estimate the parameters of the mass

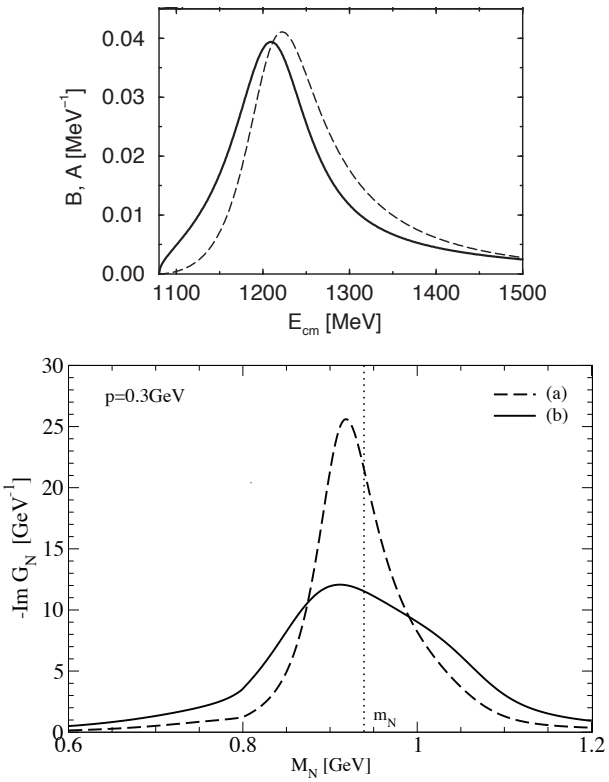

Fig. 1. Mass dependence of the Δ_{33} resonance (upper panel) and a nucleon (lower panel) found within the effective field theoretical model at a finite temperature. Upper panel: This picture is taken from the preprint arXiv:nucl-th/9710014v2 by W. Weinhold, B. Friman and W. Nörenberg, which is published in Ref. [39]. Dashed curve denotes the mass (which is the energy E_{cm} in the resonance center-of-mass frame) attenuation of the Δ_{33} resonance with vacuum mass and width, while the solid curve corresponds to the low-density approximation suggested in [39]. Lower panel: This figure is taken from the preprint arXiv:nucl-th/0407050v2 by H. van Hees and R. Rapp, which is published in Ref. [40]. As one can see from the original figure caption, the authors of Ref. [40] claim that the nucleons which are supposed to fly directly to a detector after the thermal FO, i.e. after a complete decoupling of the system, still do not have the vacuum mass and vacuum width

attenuation from the lattice QCD data [16, 17] and from the experimental Regge trajectories of heavy mesons [27].

3. Fit of Particle Ratios

The fitting procedure and the choice of particle yield ratios are the same, as suggested in [20, 21] and successfully used in [22–24]. To study the effect of the Gaussian width on the chemical FO, we choose

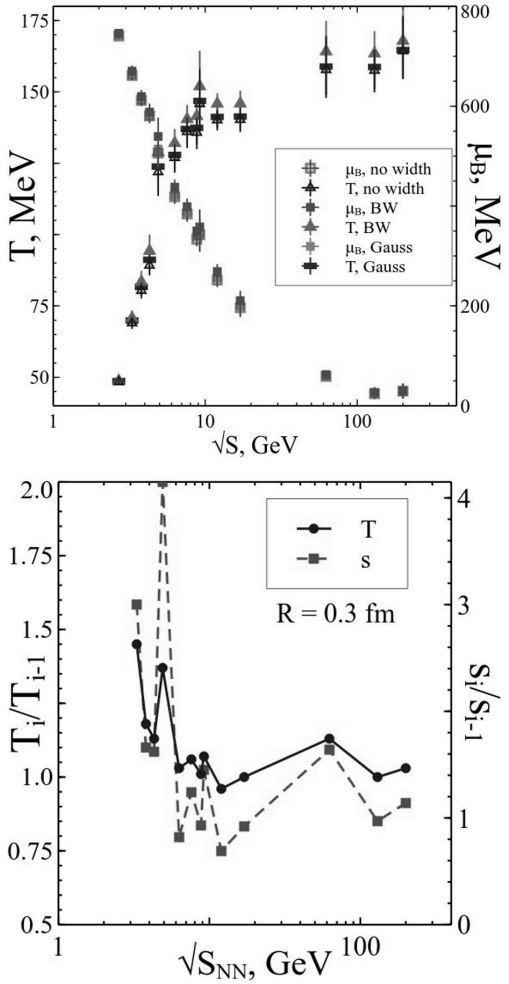

Fig. 2. Upper panel: Center-of-mass energy $\sqrt{s_{NN}}$ dependence of the chemical FO temperature $T^{\rm FO}$ and the baryonic chemical potential $\mu_B^{\rm FO}$ for three versions of the HRGM: with the Breit–Wigner width, with a vanishing width, and with the Gaussian width. Lower panel: Ratio of chemical FO temperatures $T^{\rm FO}(\sqrt{s_{NN}(i)})/T^{\rm FO}(\sqrt{s_{NN}(i-1)})$ and the ratio of entropy densities $s^{\rm FO}(\sqrt{s_{NN}(i)})/s^{\rm FO}(\sqrt{s_{NN}(i-1)})$ for two subsequent energies of collision ($i \geq 2$) are shown for the HRGMG. The lines connected the symbols are given to guide the eyes

the basic formulation of the HRGM outlined in [22] for the equal hard-core radii of all hadrons $R = 0.3$ fm, which correspond to the excluded volume $b \simeq 0.45$ fm^3.

For the AGS center-of-mass collision energy range $\sqrt{s_{NN}} = 2.7$–4.9 GeV, the used experimental data [44, 45] (pions), [46, 47] (proton), [45] (kaons), [48–51] (strange hyperons) and [52] (ϕ mesons) are well-known. As in our previous analysis [22–24] for the SPS center-of-mass collision energy range $\sqrt{s_{NN}} = 6.3$–17 GeV, we mainly concentrate on the NA49 Collaboration data [53–58], which traditionally are the most difficult to be reproduced for the HRGM. The measured data at the RHIC energies $\sqrt{s_{NN}} = 62.4, 130$, and 200 GeV are available from several experiments, but since the most data agree with each other well, we employ only the STAR data [59–64]. More details on the fitting procedure can be found in [22–24].

As one can see from the upper panel of Fig. 2, the chemical FO temperature $T^{\rm FO}$ and the baryonic chemical potential $\mu_B^{\rm FO}$ of the present model, which is called the HRGMG hereafter for convenience, are more close to the HRGM with a zero width (HRGM0) than to the HRGM with the Breit–Wigner mass attenuation (HRGMBW). Moreover, the deviation of the chemical FO temperatures obtained within HRGMG and within HRGMBW slowly grows with increase of the collision energy, but their difference, 6 MeV, does not. From the lower panel of Fig. 2, it is clearly seen that, in the narrow range of collision energies $\sqrt{s_{NN}} = 4.3$–4.9 GeV, the chemical FO temperature $T^{\rm FO}$ increases by about 1.35 times, while the entropy density at the chemical FO in this case jumps by about 4.2 times! A similar picture is seen in Fig. 3 for the pressure $p^{\rm FO}$ and the energy density $\varepsilon^{\rm FO}$ at the chemical FO. We would like to note that the quantities $s^{\rm FO}$, $p^{\rm FO}$, and $\varepsilon^{\rm FO}$ demonstrate a remarkable irregularity in the narrow range of collision energies $\sqrt{s_{NN}} = 4.3$–4.9 GeV. Thus, from Figs. 2 and 3, one can see that, for the HRGMG, the chemical FO pressure increases by 5 times, the energy density jumps by about 4.75 times, while the chemical FO temperature changes by about 1.35 times, when the collision energy increases from $\sqrt{s_{NN}} = 4.3$ GeV to $\sqrt{s_{NN}} = 4.9$ GeV, i.e., it grows by about 14% only. In other words, the quantities $s^{\rm FO}/(T^{\rm FO})^3$ and $p^{\rm FO}/(T^{\rm FO})^4$, which usually characterize the number of effective degrees of freedom, increase, by about 1.67 and 1.5 times, respectively, while the collision energy changes by about 14%. For the HRGMBW and for the unrealistic HRGM0, the results are very similar, although the pressure and the energy density obtained by the HRGMBW for the corresponding values of the collision energy are essentially larger than the ones found by the HRGMG. In Section 4, it is shown that the main reason for the stronger

HRGMBW pressure compared to the HRGMG one is due to the width parametrization.

Note that a similar behavior of $T^{\rm FO}$ and a large decrease of the chemical FO volume in this energy range were found in [20] for the HRGM with a vanishing width. However, the authors of [20] never discussed the strong irregularities in the chemical FO pressure and the energy density and their reduced values $p^{\rm FO}/(T^{\rm FO})^4$ and $\varepsilon^{\rm FO}/(T^{\rm FO})^4$. It is necessary to point out that the minimum of the chemical FO volume reached at $\sqrt{s_{NN}} = 4.9$ GeV is recently explained [65] within the shock adiabat model of central nuclear collisions. In accordance with the present framework, this minimum of the chemical FO volume corresponds to the QG phase formation [65].

It is interesting that the irregularities found here are also accompanied by the irregularity in the $\sqrt{s_{NN}}$ dependence of the Strangeness Horn [66], i.e., the multiplicity ratio K^+/π^+. As one can see from the straight lines in the upper panel of Fig. 4, there is a strong change of the K^+/π^+ ratio slope in the energy range $\sqrt{s_{NN}} \simeq 4.3 - 4.9$ GeV. Of course, the existing large error bars do not allow us to locate the transition point with high accuracy, but we can hope for that the future experiments will provide us with essentially smaller errors, which will allow one, in turn, to make more definite conclusions. It is odd that all found dependences of thermodynamic quantities at the chemical FO were assumed from the very beginning to be continuous and smooth [20, 67]. Probably, such an attitude did not allow other researchers to find out these irregularities. In contrast to the traditional assumptions, Figs. 1, 2 and 3 clearly demonstrate that the $\sqrt{s_{NN}}$ dependence of the chemical FO parameters $T^{\rm FO}$, $p^{\rm FO}$ and $\varepsilon^{\rm FO}$ has a discontinuity. Therefore, in order to distinguish our concept of chemical FO from the previous findings with a smooth functional dependences, we name it as *the non-smooth chemical FO*.

In order to parametrize the functions $T^{\rm FO}(\sqrt{s_{NN}})$ and $T^{\rm FO}(\mu_B^{\rm FO})$ for the non-smooth chemical FO, let us introduce, for convenience, the functions

$$c_-(x,a,b) = \frac{1}{1+e^{(a-x)/b}} = \frac{1}{2}\left(1+\tanh\frac{x-a}{2b}\right), \quad (8)$$

$$c_+(x,a,b) = \frac{1}{1+e^{(x-a)/b}} = \frac{1}{2}\left(1-\tanh\frac{x-a}{2b}\right). \quad (9)$$

Such functions, sigmoids, are well known in physics, because they represent Fermi–Dirac distributions. In the limit of small values of parameter b, they become $c_+(x,a,b)|_{b\to 0} = \theta(a-x)$ and $c_-(x,a,b)|_{b\to 0} = \theta(x-a)$, where $\theta(x)$ is the usual Heaviside function. For finite b, the functions (8) and (9) cut the x values for $x > a$ and $x < a$, respectively. The width of a smooth cut transition is of about $2b$.

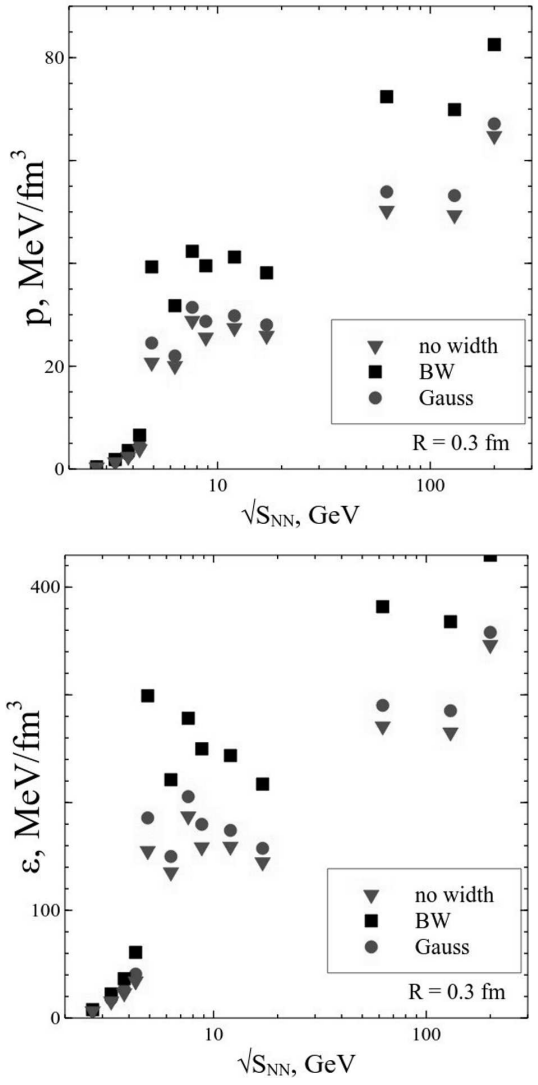

Fig. 3. Center-of-mass energy $\sqrt{s_{NN}}$ dependence of the chemical FO pressure $p^{\rm FO}$ (left) and the energy density $\varepsilon^{\rm FO}$ (right) for three versions of the HRGM: with the Breit–Wigner width, with a vanishing width, and with the Gaussian width. Both quantities demonstrate a huge jump in the narrow range of collision energies $\sqrt{s_{NN}} = 4.3$–4.9 GeV. The reason for why the Gaussian and zero-width pressures are smaller than the Breit–Wigner one is thoroughly analyzed in Sect. 4

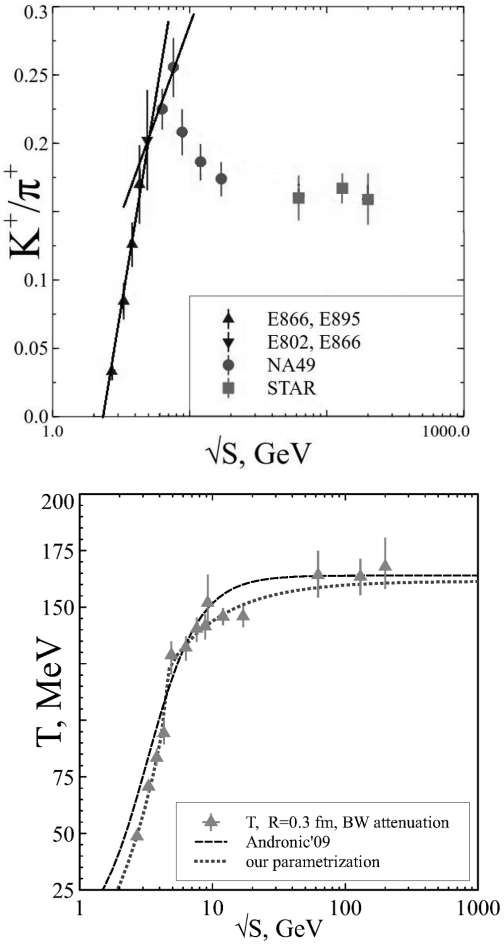

Fig. 4. Upper panel: The center-of-mass energy $\sqrt{s_{NN}}$ dependence of the experimental K^+/π^+ ratio (Strangeness Horn). The straight lines indicate the slope change from 0.667 for $\sqrt{s_{NN}} \in [2.7; 4.9]$ GeV to 0.275 for $\sqrt{s_{NN}} \in [4.3; 7.6]$ GeV. Lower panel: The chemical FO temperature $T^{\rm FO}$ for the HRGMBW as a function of the center-of-mass energy $\sqrt{s_{NN}}$ and its two theoretical representations. The dashed curve corresponds to Eq. (10), while the dotted curve represents Eq. (12)

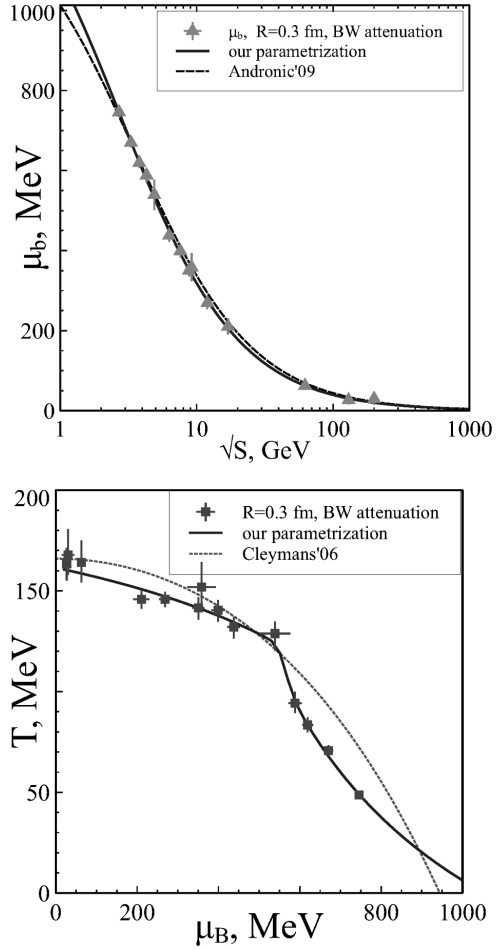

Fig. 5. Upper panel: The baryonic chemical potential $\mu_B^{\rm FO}$ at the chemical FO as a function of the center-of-mass energy $\sqrt{s_{NN}}$ for the HRGMBW. The dashed and solid curves are, respectively, defined by Eqs. (11) and (13). Lower panel: The chemical FO temperature $T^{\rm FO}$ as a function of the baryonic chemical potential at FO $\mu_B^{\rm FO}$ for the HRGMBW. The solid and dotted curves are, respectively, defined by system (12), (13) and by Eq. (14)

First, let us discuss some popular parametrizations for $T^{\rm FO}(\sqrt{s_{NN}})$ and $\mu_B^{\rm FO}(\sqrt{s_{NN}})$. In 2009, Andronic and collaborators in [21] considered a slightly different particle spectrum in their HRGM developed in [20] (in particular, they introduced a σ-meson) in order to improve their results of Ref. [20] on the pion multiplicity and, hence, on the Strangeness Horn. Their thermal parameters have altered, but only very slightly. In [21], they suggested the following parametrizations for $T^{\rm FO}(\sqrt{s_{NN}})$ and $\mu_B^{\rm FO}(\sqrt{s_{NN}})$:

$$T^{\rm FO}[\text{MeV}] = \frac{T_A^{\rm lim}}{1+\exp\left[2.60-\ln(\sqrt{s_{NN}})/0.45\right]} = T_A^{\rm lim}\, c_-(\ln(\sqrt{s_{NN}}), 1.17, 0.45), \quad (10)$$

$$\mu_B^{\rm FO}[\text{MeV}] = \frac{a_A}{1+b_A\sqrt{s_{NN}}}. \quad (11)$$

Here, $T_A^{\rm lim} = 164 \pm 4$ MeV, $a_A = 1303 \pm 120$ MeV, $b_A = 0.286 \pm 0.049$ GeV^{-1}, and $\sqrt{s_{NN}}$ is given

in GeVs. The functions $T^{\rm FO}(\sqrt{s_{NN}})$ (10) and $\mu_B^{\rm FO}(\sqrt{s_{NN}})$ (11) are, respectively, shown by the dashed curves in the lower panel of Fig. 4 and in the upper panel of Fig. 5. As one can see from the upper panel of Fig. 5, the function $\mu_B^{\rm FO}(\sqrt{s_{NN}})$ (11) rather well describes the chemical FO points of the HRGMBW, but the function $T^{\rm FO}(\sqrt{s_{NN}})$ (10) describes well only the points with the collision energies $\sqrt{s_{NN}} = 9.2, 62.4, 130$, and 200 GeV, while the other points, especially for $\sqrt{s_{NN}} \leq 4.9$ GeV, are poorly reproduced.

We suggest another type of parametrization, which aims at a precise description of the chemical FO points. We note that the behavior of $T^{\rm FO}(\sqrt{s_{NN}})$ is qualitatively different in the regions $\sqrt{S} < 4.5$ GeV and $\sqrt{S} > 4.5$ GeV. Therefore, the dependences $T^{\rm FO}(\sqrt{s_{NN}})$ and $\mu_B^{\rm FO}(\sqrt{s_{NN}})$ found by the HRGMBW are parametrized in the following way:

$$T^{\rm FO}[\text{MeV}] = (T_{1O} + T_{2O}\sqrt{s_{NN}})c_+(\sqrt{s_{NN}}, 4.5, 0.1) +$$

$$+ (T_{3O}/\sqrt{s_{NN}} + T_O^{\rm lim})c_-(\sqrt{s_{NN}}, 4.5, 0.1), \qquad (12)$$

$$\mu_B^{\rm FO}[\text{MeV}] = \frac{a_O}{(1 + b_O\sqrt{s_{NN}})}. \qquad (13)$$

Here, the functions c_+ and c_- are used to make a smooth transition from one kind of the $\sqrt{s_{NN}}$ behavior to another. The fitting results in the following values of the coefficients: $T_{1O} = -34.4$ MeV, $T_{2O} = 30.9$ MeV/GeV, $T_{3O} = -176.8$ GeV$\cdot$MeV, and $T_O^{\rm lim} = 161.5$ MeV with $\chi^2/\text{dof} = 6.6/10$ for $T^{\rm FO}(\sqrt{s_{NN}})$ (12). The parametrization for $\mu_B^{\rm FO}(\sqrt{s_{NN}})$ (13) is the same as in (11), but the coefficients are different, i.e., $a_O = 1481.6$ MeV, $b_O = 0.365$ GeV^{-1}. For parametrization (13), we found $\chi^2/\text{dof} = 2.3/12$. The resulting curve $T^{\rm FO}(\mu_B^{\rm FO})$ (see the solid curve in the lower panel of Fig. 5) has $\chi^2 = 4.9$ for 14 data points, and it does not contain any free parameter. Note that, for the chemical FO curves of the HRGMG, the parameters entering Eqs. (12) and (13) are practically the same. Hence, we do not show these curves in the figures. From the upper panel of Fig. 2, it is easy to understand the fact that the main difference between the parameters of curves (12) and (13) corresponding to the HRGMBW and the HRGMG is in the value of $T_O^{\rm lim}$, which is by about 6 MeV smaller for the latter model. We hope that parametrizations (12) and (13) can be verified with more precise data, which will be measured in a few years on new accelerators, since the narrow range of the center-of-mass energy corresponds to a wide range of the laboratory energy.

In the lower panel of Fig. 5, we compare the resulting curve $T^{\rm FO}(\mu_B^{\rm FO})$ (solid curve) obtained in this work with the parametrization

$$T[\text{GeV}] = 0.166 - 0.139\left(\mu_B^{\rm FO}\right)^2 - 0.053\left(\mu_B^{\rm FO}\right)^4 \qquad (14)$$

suggested in [67]. Equation (14) is a fit to the chemical FO points obtained within different versions of the HRGM. Several of these HRGM analyzed in [67] take the hard core repulsion into account, but none of them includes all hadronic states and none of them considers the width of hadronic resonances in the full range of collision energies. Now, it is clear that these two approximations cause the large deviation from the results obtained in this work.

From the lower panel of Fig. 5, one can see that, at small baryonic chemical potentials, the slopes of the curves defined by Eq. (14) and by system (12), (13) are different. Note that there is no *a priori* reason to believe that the function $T^{\rm FO}(\mu_B^{\rm FO})$ should have a vanishing $\mu_B^{\rm FO}$ derivative at $\mu_B^{\rm FO} = 0$. The high-quality description of the chemical FO points provided by system (12), (13) gives evidence against such a belief.

It is worth to note that the traditional functions $T^{\rm FO}(\mu_B^{\rm FO})$ like the one given by Eq. (14), which describes the smooth dependence of chemical FO parameters, are often used in the works employing the obsolete and oversimplified versions of the HRGM. The latter versions have a very short list of hadronic states, and they do not account for the resonance decays and for their nonzero width. In fact, the vast majority of such models was never used to describe the actual experimental data, but they are employed for various "predictions". Therefore, the likelihood of such "predictions" is very low. Typical examples of such works are Refs. [68, 69], where the authors analyze the ratio of the entropy density to the cube of temperature at the chemical FO in detail, i.e. $s^{\rm FO}/(T^{\rm FO})^3$, using a smooth parametrization $T^{\rm FO}(\mu_B^{\rm FO})$ (14) (see, e.g., Fig. 4, *b* in [68]). As one can see from Fig. 4, *b* in [68], the sum of ratios $s^{\rm FO}/(T^{\rm FO})^3$ found for mesons and baryons should demonstrate a strong decrease as a function of the collision energy at $E_{\rm lab} \geq 3$ GeV, i.e, at $\sqrt{s_{NN}} \geq 2.7$ GeV. Note that such a behavior is not seen within the realistic versions of the HRGM.

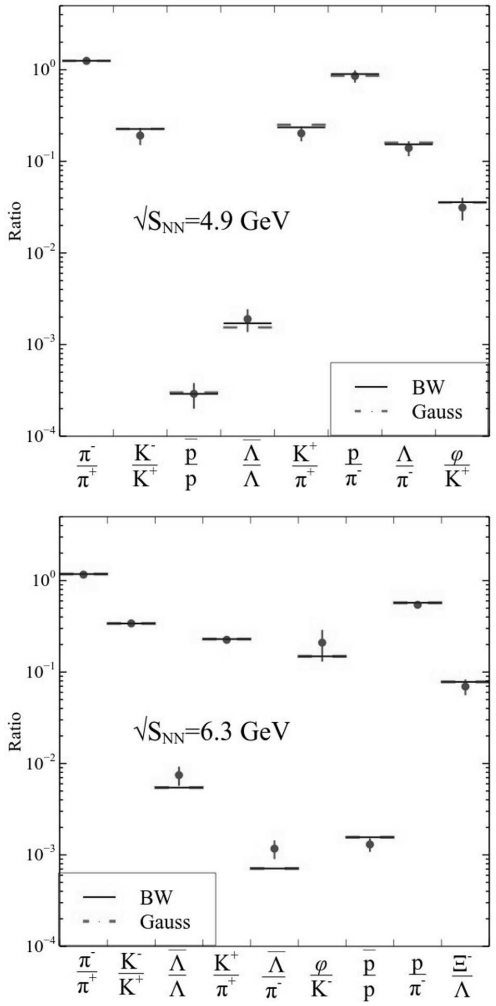

Fig. 6. Particle yield ratios described by the present HRGMG. The best fit for $\sqrt{s_{NN}} = 4.9$ GeV is obtained for $T \simeq 123.8$ MeV, $\mu_B \simeq 514.4$ MeV, $\mu_{I3} \simeq -16.75$ MeV (upper panel), whereas, for $\sqrt{s_{NN}} = 6.3$ GeV (lower panel), it is obtained for $T \simeq 127.9$ MeV, $\mu_B \simeq 421.9$ MeV, $\mu_{I3} \simeq$ $\simeq -10.9$ MeV. A yield ratio of two particles is denoted by the ratio of their respective symbols

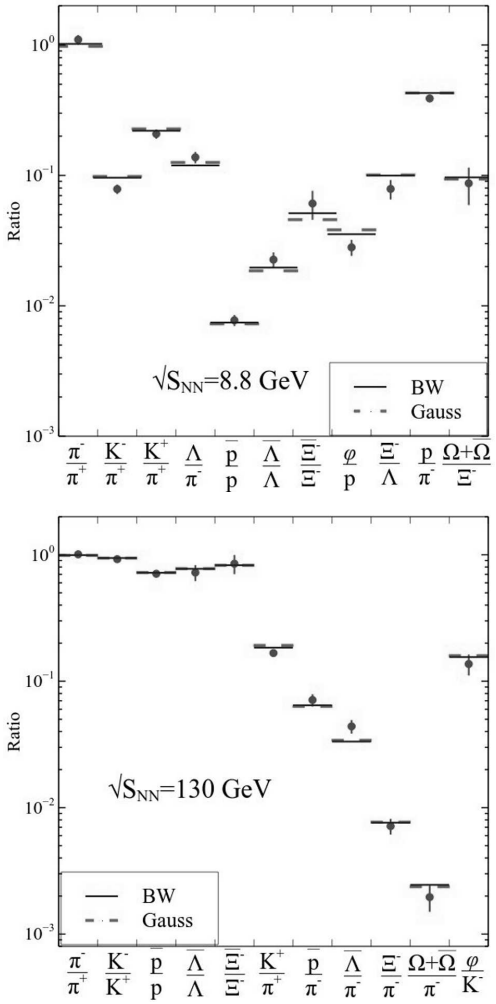

Fig. 7. Same as in Fig. 6, but for $\sqrt{s_{NN}} = 8.8$ and 130 GeV. For $\sqrt{s_{NN}} = 8.8$ GeV, the fit parameters are $T \simeq 137.4$ MeV, $\mu_B \simeq 338.5$ MeV, $\mu_{I3} \simeq 2.19$ MeV (upper panel), whereas, for $\sqrt{s_{NN}} = 130$ GeV (lower panel), one finds $T \simeq 158.7$ MeV, $\mu_B \simeq 24.93$ MeV, $\mu_{I3} \simeq 1.64$ MeV

A few selected particle yield ratios described within the HRGMG are shown in Figs. 6 and 7. From these figures, one can see that the overall fit is good, and the results of the HRGMG are almost the same as the ones found within the HRGMBW. The resulting χ^2/dof obtained for the HRGMG is $\chi^2/\text{dof} = 150.8/59 \simeq 2.56$. It is only 17 % larger than the one $\chi^2/\text{dof} = 125.5/59 \simeq 2.12$ found in the HRGMBW. From our previous experience, we know that the main part of these values of χ^2/dof should be attributed to the ratios involving the heavy strange particles [22–24] (see, e.g., the ratios Λ/π^-, $\bar{\Lambda}/\pi^-$, and ϕ/p in Figs. 6 and 7). However, in Refs. [22–24], it was also demonstrated that the quality of the fit of these problematic ratios can be essentially improved, if one uses the multicomponent hard-core repulsion [23] and introduces the strangeness enhancement factor [24]. An additional important feature of such improvements is that they practically do not affect the values of thermodynamic functions at the chemical

FO, since the variations of $T^{\rm FO}$ and $\mu_B^{\rm FO}$ are small, and the contributions of heavy strange particles into $s^{\rm FO}$, $p^{\rm FO}$ and $\varepsilon^{\rm FO}$ are almost negligible. Moreover, a close inspection of the thermodynamic quantities $s^{\rm FO}$, $p^{\rm FO}$, and $\varepsilon^{\rm FO}$ obtained within the most successful versions of the HRGM [22–24] shows that the non-smooth chemical FO is their inherent feature.

Now, we would like to clarify the question whether the found irregularities and a drastic change in the number of effective degrees of freedom seen at $\sqrt{s_{NN}} = 4.3$–4.9 GeV are related to the deconfinement transition from a hadron gas to a QG plasma. Although the famous irregularities known as the Kink [70], the Strangeness Horn [66], and the Step [71] are observed at a somewhat higher energy $\sqrt{s_{NN}} \geq 7.63$ GeV, we have to point out that, until the more convincing signals of the deconfinement phase transition will be found, there is no reason to believe that the mentioned irregularities [66, 70, 71] are, indeed, the signals of the onset of a deconfinement. Moreover, despite the widely spread claims [72], the absence of a solid theoretical backup of these irregularities [66,70,71] does not allow one to consider them as the convincing signals of the onset of a deconfinement. Furthermore, a successful description of every tiny detail of the Strangeness Horn achieved recently within the HRGMBW [24] tells us that there are no associated irregularities in the thermodynamic quantities at and above the corresponding value of collision energy $\sqrt{s_{NN}} = 7.63$ GeV. Therefore, until the more convincing signals will be found, the irregularities at $\sqrt{s_{NN}} = 4.3$–4.9 GeV reported above can be also considered as the signals of the deconfinement phase transition. Moreover, such a conclusion was essentially enhanced recently by the shock adiabat model of central nuclear collisions [65], which connects the jump of the number of effective degrees of freedom p/T^4 at collision energies $\sqrt{s_{NN}} = 4.3$–4.9 GeV with the formation of QG plasma at $\sqrt{s_{NN}} \simeq$ $\simeq 4.67$ GeV.

In contrast to some general speculations [72] on a possible source of the above-mentioned irregularities [66, 70, 71], the non-smooth chemical FO has an additional theoretical backup provided by the FWM [16, 17, 27]. The FWM [16, 17] is able to successfully describe a variety of the lattice QCD thermodynamics data [73–75] at vanishing baryonic chemical potential. In addition, its predictions for the Regge trajectories of non-strange and strange mesons [27] were successfully confirmed by the thorough analysis of both the real and imaginary parts of the leading Regge trajectories [37] of ρ_{J--}, ω_{J--}, a_{J++}, and f_{J++} mesons for the spin values $J \leq 6$ and the ones of K^*_{JP} mesons of isospin $\frac{1}{2}$, parity $P = (-1)^J$, and spin values $J \leq 5$. One of the most important predictions of the FWM [16, 17] is that, at the vanishing baryonic chemical potential, the QG bags are strongly suppressed (by a factor of fifteen-sixteen orders of magnitude) compared to nucleons up to temperatures of a half of the Hagedorn temperature, i.e., $T_{\rm suppr} \simeq \frac{1}{2} T_{\rm H}$. Since, for the different lattice QCD data analyzed in [17], the Hagedorn temperature varies from $T_{\rm H} \simeq 160$ MeV to $T_{\rm H} \simeq 188$ MeV, the corresponding range of the suppression temperatures is $T_{\rm suppr} \simeq 80$–95 MeV. It is remarkable that the chemical FO temperatures at $\sqrt{s_{NN}} = 4.3$ GeV are $T_{\rm FO} \simeq 90$–95 MeV, while, at $\sqrt{s_{NN}} = 4.9$ GeV, they are $T_{\rm FO} \simeq 123$–128 MeV. In other words, according to the FWM [16,17] at $\sqrt{s_{NN}} = 4.9$ GeV, the QG bags can be formed. Of course, it is unclear at present whether the QG bags are formed at the chemical FO stage as the metastable states of finite systems created in nuclear collisions or they are formed at earlier stages of a collision.

One may dispute our argument concerning the application of the results obtained within the FWM at the vanishing densities to high baryonic ones. We, however, should point out that the density of states of QG bags with zero baryonic charge, i.e. meson-like bags, cannot depend on the baryonic charge of the system. The question about the baryonic density dependence of the mass density and the width of meson-like QG bags cannot be directly answered at the moment. Nevertheless, one should account for two facts. The first of them is that the FWM establishes a strict proportionality between the pseudocritical temperature $T_{\rm pc}$ at the cross-over and the Hagedorn temperature $T_{\rm H} = c\, T_{\rm pc}$ with the constant $c \in [0.92$–$0.98]$, which weakly depends on the number of quark flavors and the number of colors. The second fact is that the lattice QCD thermodynamics shows a very weak dependence of $T_{\rm pc}$ on the baryonic chemical potential μ_B [76]:

$$\frac{T_{\rm pc}(\mu_B)}{T_{\rm pc}(0)} = 1 - 0.0066(7) \left(\frac{\mu_B}{T_{\rm pc}(\mu_B)}\right)^2.$$

Therefore, we conclude from these facts that the possible μ_B dependences of the mass density and the

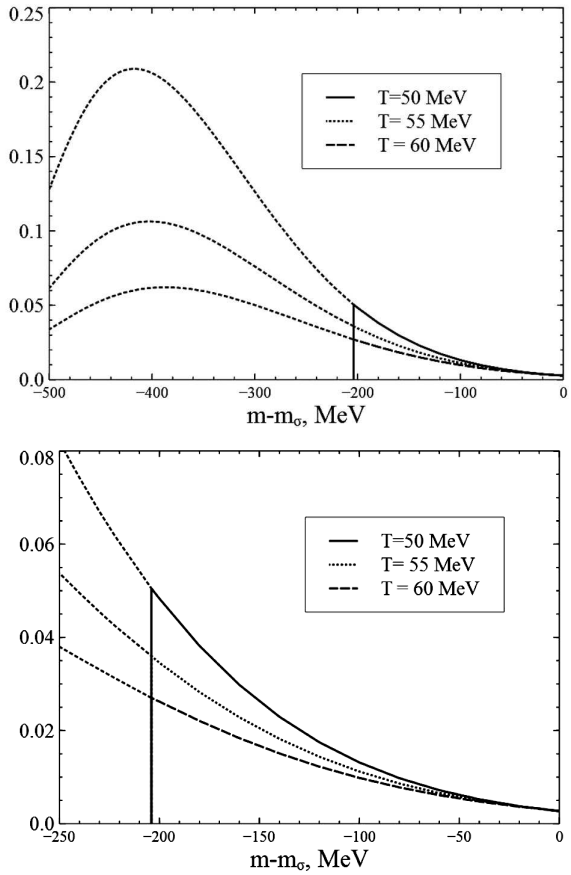

Fig. 8. Temperature dependence of the mass distribution $f_k^G(m)/\phi(m_\sigma, T)$ (in units of 1/MeV, see Eq. (16)) for a σ-meson with the mass $m_\sigma = 484$ MeV, the width $\Gamma_\sigma = 510$ MeV [79], and $M_\sigma^{\rm Th} = 2\,m_\pi \simeq 280$ MeV. In the upper panel, the short dashed curves below the two-pion threshold (vertical line at $m - m_\sigma = -204$ MeV) show the mass attenuation which does not contribute into the particle density (16). From the lower panel, one can see the effect of the wide resonance sharpening near the threshold, i.e., the appearance of a narrow peak in the resulting mass distribution on the right-hand side of the threshold, which resembles an icy slide. For different temperatures, this mass attenuation is shown by the solid, short dashed, and long dashed curves. The σ-meson effective width was found numerically from these mass attenuations: $\Gamma_\sigma^{app}(T = 50\,{\rm MeV}) \simeq 62.5$ MeV, $\Gamma_\sigma^{app}(T = 55\,{\rm MeV}) \simeq$ $\simeq 71.5$ MeV and $\Gamma_\sigma^{app}(T = 60\,{\rm MeV}) \simeq 82.5$ MeV

width of meson-like QG bags should be very weak as well. Thus, our previous estimates of the Hagedorn temperature value of meson-like QG bags should be valid at nonzero μ_B values as well.

In the next section, we discuss the question how one can observe the meson-like QG bags.

4. An Apparent Width of Wide Resonances and Meson-Like QG Bags

Now, we would like to analyze the apparent width of wide resonances and meson-like QG bags in a thermal environment. The typical term of the k-resonance that enters into the mass spectrum (1) of the HRGMG is as follows:

$$F_k(\sigma_k) \equiv g_k \int\limits_0^\infty dm \frac{\Theta\left(m - M_k^{\rm Th}\right)}{N_k(M_k^{\rm Th})} \exp\left[-\frac{(m_k - m)^2}{2\sigma_k^2}\right] \times$$
$$\times \int \frac{d^3p}{(2\pi)^3} \exp\left[-\frac{\sqrt{p^2 + m^2}}{T}\right]. \qquad (15)$$

The notations used in (15) are the same as in Eqs. (2)–(4). Evidently, the term $F_k(\sigma_k)$ for the narrow resonances converts into the usual thermal density of particles, i.e., as $\sigma_k \to 0$, one has $F_k \to$ $\to g_k\,\phi(m_k, T)$.

The momentum integral in (15) can be written, by using the non-relativistic approximation $\phi(m, T) \simeq$ $\simeq \left[\frac{m\,T}{2\,\pi}\right]^{\frac{3}{2}} \exp\left[-\frac{m}{T}\right]$. Then, to simplify the mass integration in (15), one can make the full square in it from the powers of $(m_k - m)$ and get

$$F_k(\sigma_k) \equiv g_k \int\limits_0^\infty dm\, f_k^G(m) \simeq \tilde{g}_k \int\limits_0^\infty dm\, \frac{\Theta\left(m - M_k^{\rm Th}\right)}{N_k(M_k^{\rm Th})} \times$$
$$\times \exp\left[-\frac{(\tilde{m}_k - m)^2}{2\,\sigma_k^2}\right] \left[\frac{m\,T}{2\pi}\right]^{3/2} \exp\left[-\frac{m_k}{T}\right], \qquad (16)$$

where the following notations for the effective resonance degeneracy $\tilde{g}_k$ and the an effective resonance mass $\tilde{m}_k$

$$\tilde{g}_k \equiv g_k \exp\left[\frac{\sigma_k^2}{2\,T^2}\right] = g_k \exp\left[\frac{\Gamma_k^2}{2\,Q^2\,T^2}\right], \qquad (17)$$

$$\tilde{m}_k \equiv m_k - \frac{\sigma_k^2}{T} = m_k - \frac{\Gamma_k^2}{Q^2\,T} \qquad (18)$$

are used. From Eq. (16), one can see that the presence of the width, firstly, can strongly modify the degeneracy factor g_k and, secondly, it may essentially shift the maximum of the mass attenuation toward the threshold or even below it. There are two corresponding effects, which we named as *the near threshold thermal resonance enhancement* and *the near threshold resonance sharpening*. These effects formally appear due to the same reason as the famous Gamow window

The parameters of several hadronic resonances together with their decay channels that are used to determine the quantities β_k and T^+_{kG}. The last two columns show the corresponding effective width at the temperature $T = 50$ MeV found, respectively, numerically from Eq. (15) and analytically from Eq. (19), when it can be applied

Hadron	m_k (MeV)	Γ_k (MeV)	Decay channel	$M_k^{\rm Th}$ (MeV)	β_k	T^+_{kG} (MeV)	exact $\Gamma_k^{\rm app}$ (MeV)	approx. $\Gamma_k^{\rm app}$ (MeV)
σ-meson	484	510	$\sigma \to \pi\pi$	280	0.942	91.9	62.5	67.3
P_{33}	1232	120	$\Delta \to \pi N$	1080	2.98	11.6	43.5	N/A
P_{11}	1440	350	$N \to \pi N$	1080	2.42	38.74	129.5	N/A
P_{33}	1600	350	$\Delta \to \pi\Delta$	1372	1.53	50.4	68.7	80.8
P_{33}	1600	350	$\Delta \to \pi N$	1080	3.5	30.3	280.0	N/A
G_{17}	2190	500	$\Delta \to \rho N$	1710	2.26	57.8	74.6	81.8

for the thermonuclear reactions in stars [77, 78]: just above the resonance decay threshold, the integrand in (16) is a product of two functions of the virtual resonance mass m, namely, the Gaussian attenuation is an increasing function of m, while the Boltzmann exponent strongly decreases above the threshold. The resulting attenuation of their product has a maximum, whose shape, in contrast to the usual Gamow window, can be extremely asymmetric due to the presence of the threshold. Indeed, as one can see from Fig. 8, the resulting mass attenuation of a resonance can acquire the form of a sharp narrow peak, which closely resembles an icy slide. Below, we discuss these two effects in some details. Qualitatively the same effects appear, if one uses the Breit–Wigner resonance mass attenuation in (16) instead of the Gaussian one (see below).

From the definitions of the effective resonance mass (18) and the effective resonance degeneracy (17), one can see that the effects of their change are strong for $T \ll \sigma_k$. This can be clearly seen from Fig. 8, which demonstrates both of the above effects at low temperatures for the σ-meson. A simple analysis shows that the effect of resonance sharpening is strongest, if the threshold mass is shifted to the convex part of the Gaussian distribution in (16), i.e., for $M_k^{\rm Th} \geq \tilde{m}_k$ or for the temperatures T below $T_k^+ \equiv \frac{\sigma_k^2}{m_k - M_k^{\rm Th}} \equiv \frac{\sigma_k}{\beta_k}$. To demonstrate the effect of the width sharpening, we list a few typical examples for baryons in Table. For $T < T_k^+$ and for $m > M_k^{\rm Th}$, the Gaussian mass distribution in (16) can be safely approximated as $\exp\left[-\frac{(\tilde{m}_k - m)^2}{2\,\sigma_k^2}\right] \approx$ $\approx \exp\left[-\frac{(\tilde{m}_k - M_k^{\rm Th})^2}{2\,\sigma_k^2} - \frac{(\tilde{m}_k - M_k^{\rm Th})}{\sigma_k^2}(m - M_k^{\rm Th})\right]$. Now recalling the standard definition of the width for the function $f(x) = \Theta(x)\,{\rm Const}\,\exp[-b\,x]$, one obtains the temperature-dependent resonance effective width near the threshold as

$$\Gamma^{\rm app}_{kG}(T) \simeq \frac{\ln(2)}{\frac{1}{T} - \frac{\beta_k}{\sigma_k}} \equiv \frac{\ln(2)}{\frac{1}{T} - \frac{1}{T^+_{kG}}}, \qquad (19)$$

since, for such a distribution function $f(x)$, one gets $f(\ln(2)/b) = f(0)/2$. Note that, in evaluating (19), we neglected the additional $m^{1.5}$-dependence in (16), but one can readily check that such a correction is numerically small. The rightmost column in Table demonstrates that Eq. (19) provides, indeed, an accurate estimate for $T < T^+_{kG}$. To some extent, the results of Table justify the usage of the σ-meson in the field theoretical models based on the well-known σ-model for temperatures below $T^+_\sigma \simeq 92$ MeV. Of course, the present approach, which is developed for the chemical FO stage, when the inelastic reactions are ceased to exist except for resonance decays, cannot be applied for earlier stages of heavy ion collisions. However, we would like to recall that the inclusion of the large width of the σ-meson in the field theoretical models of the strongly interacting matter equation of state is very necessary. From the above analysis, one can see that the inclusion of the large width can generate some new important physical effects like the wide resonance sharpening in a thermal medium.

From Fig. 9, one can see that the resonance enhancement can be, indeed, huge for wide ($\Gamma \geq$ ≥ 450 MeV) and medium wide ($\Gamma \simeq 300$–400 MeV) resonances. This effect naturally explains enhancements of the hadronic pressure and the energy den-

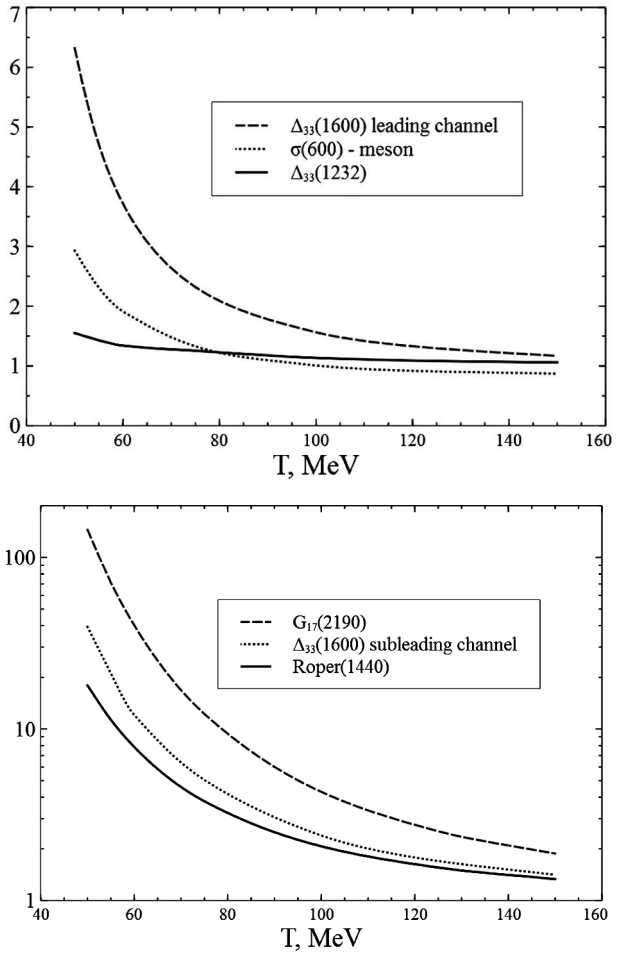

Fig. 9. Temperature dependence of the resonance enhancement factor $R_G = \frac{F_k(\sigma_k)}{g_k\,\phi(m_k,T)}$ for the HRGMG. The resonance enhancement factor R_G is shown for the hadronic resonance decays given in Table. At low temperatures, the enhancement factor of wide resonances can be huge

sity at the chemical FO compared to the zero width case (see Fig. 3). It is appropriate here to define the apparent width for the Breit–Wigner mass attenuation. Replacing the Gaussian mass attenuation in (15) by the Breit–Wigner one, we obtain, instead of the function $f_k^G(m)$ in (16),

$$f_k^{\rm BW}(m) \simeq \frac{\Theta\left(m - M_k^{\rm Th}\right)}{N_k^{\rm BW}(M_k^{\rm Th})}\,\frac{m^{-B}}{(m_k-m)^2+\frac{\Gamma_k^2}{4}}\,\times$$
$$\times\left[\frac{m\,T}{2\pi}\right]^{3/2}\exp\left[-\frac{m}{T}\right], \qquad (20)$$

$$N_k^{\rm BW}(M_k^{\rm Th}) \equiv \int\limits_0^\infty dm\,\frac{\Theta\left(m - M_k^{\rm Th}\right)\,m^{-B}}{(m_k-m)^2+\frac{\Gamma_k^2}{4}}. \qquad (21)$$

Here, we introduced an additional mass dependence factor m^{-B} for convenience ($B = \text{const}$). Calculating the mass derivative of $\ln(f_k^{\rm BW}(m))$ for $m > M_k^{\rm Th}$, one finds:

$$\frac{d}{dm}\ln(f_k^{\rm BW}(m)) \simeq$$
$$\simeq -\frac{1}{T}\;-\;\frac{2(m-m_k)}{(m_k-m)^2+\frac{\Gamma_k^2}{4}}\;+\;\frac{\frac{3}{2}-B}{m}. \qquad (22)$$

Similarly to the case of the Gaussian width, relation (22) yields the apparent width in the Breit–Wigner case as

$$\Gamma_{k\rm BW}^{\rm app} \simeq -\frac{\ln(2)}{\frac{d}{dm}\ln(f_k^{\rm BW}(M_k^{\rm Th}+0))} = \frac{\ln(2)}{\frac{1}{T}\;-\frac{1}{T_{k\rm BW}^+}}, \qquad (23)$$

$$\frac{1}{T_{k\rm BW}^+} \simeq \frac{2\,\beta_k}{\sigma_k\left(\beta_k^2+\frac{Q^2}{4}\right)} + \frac{\frac{3}{2}-B}{M_k^{\rm Th}} \equiv$$
$$\equiv \frac{2}{T_{kG}^+\left(\beta_k^2+\frac{Q^2}{4}\right)} + \frac{\frac{3}{2}-B}{M_k^{\rm Th}}, \qquad (24)$$

where, on the last step of the evaluation, we used the same notations as in Eq. (19). From Eq. (24), one can deduce two conclusions. First, for $M_k^{\rm Th} \gg T$, the last term on the right-hand side of (24) can be safely neglected, if $O(\frac{3}{2}-B) \sim 1$. This fact shows that the power-like deformations of the Breit–Wigner attenuation cannot affect the apparent width (23). This is the main reason why the tiny deformations of the resonance mass attenuation discussed earlier with respect to claims of Ref. [39] should not be taken seriously, since they are much weaker than the effect of a thermal environment clearly seen in Eqs. (19) and (23).

Second, for $\beta_k \geq 1$, one finds that $2\left(\beta_k^2+\frac{Q^2}{4}\right)^{-1} \simeq$ $\simeq \frac{2}{\left(\beta_k^2+1.4\right)} < 1$. From the last inequality, we find two following important inequalities:

$$\frac{1}{T_{k\rm BW}^+} \;<\; \frac{1}{T_{kG}^+} \quad\Rightarrow\quad \Gamma_{k\rm BW}^{\rm app}(T) \;<\; \Gamma_{kG}^{\rm app}(T). \qquad (25)$$

The inequalities above are valid for $T < T_{kG}^+$. They show that, compared to the Gaussian width parametrization, the range of mass states contributing into the pressure defined by the Breit–Wigner

mass attenuation of wide resonances is closer to the threshold. In order to demonstrate how the apparent width of wide resonances behaves at higher temperatures, it is instructive to study the enhancement factor for the Breit–Wigner and Gaussian attenuations in some details. For this purpose, it is convenient to rewrite the enhancement factor $R = \frac{F_k(\sigma_k)}{\phi(m_k,T)}$ of heavy resonances in the non-relativistic approximation ($m_k \gg T$) as

$$R_G(\beta,t) = \int\limits_{-\beta}^{\infty} \frac{dx\,[1+s\,x]^{\frac{3}{2}}\,\exp\left[-\frac{x^2}{2}-\frac{x}{t}\right]}{\int\limits_{-\beta}^{\infty} dy \exp\left[-\frac{y^2}{2}\right]}, \qquad (26)$$

$$R_{\rm BW}(\beta,t) = \int\limits_{-\beta}^{\infty} \frac{dx\,[1+s\,x]^{\frac{3}{2}}\,\exp\left(-\frac{x}{t}\right)}{\left(x^2+\frac{Q^2}{4}\right)\int\limits_{-\beta}^{\infty}\frac{dy}{\left(y^2+\frac{Q^2}{4}\right)}}, \qquad (27)$$

where, for a resonance of the k-th sort, the parameters are defined as follows: s stays for $s_k \equiv \frac{\sigma_k}{m_k}$, while β stays for β_k, and the reduced temperature t is given in terms of the Gaussian resonance width σ_k as $t_k \equiv \equiv T/\sigma_k$. The x- and y-integrations in Eqs. (26) and (27) are performed over the dimensionless variable $(m-m_k)/\sigma_k$.

The enhancement factors (26) and (27) demonstrate a strong dependence on β and t and a weak one on the variable s. Therefore, we depict the results for some typical values of β_k and t_k in Figs. 10 and 11, while fixing the s value to $s = s_k \simeq 0.1032$, which corresponds to the Roper resonance. Actually, the parameters chosen for the upper and lower panels of Fig. 10 are, respectively, very close to the parameters of the Roper resonance (compare $\beta = 2.5$ in Fig. 10 and $\beta_{\rm Roper} \simeq 2.42$) and the P_{33} resonance (compare $s = 0.1032$ in Fig. 10 and $s_{P_{33}} \simeq 0.093$), which decays into a pion and a nucleon (see Table). Therefore, in case of the Roper resonance, the actual temperature of the upper panel of Fig. 10 is about 149 MeV, while, for the P_{33} resonance with $\beta_{P_{33}} \simeq 3.5$, its lower panel corresponds to a temperature of about 75 MeV.

As one can see from the upper panel of Fig. 10, the Breit–Wigner mass attenuation is more narrow than the Gaussian one, while the lower panel of this figure corresponds to the opposite case. Nevertheless, as is clear from Fig. 11, both of the cases correspond to the inequality $R_{\rm BW} > R_G$. In order to understand this inequality, we note that the normalized Breit–Wigner

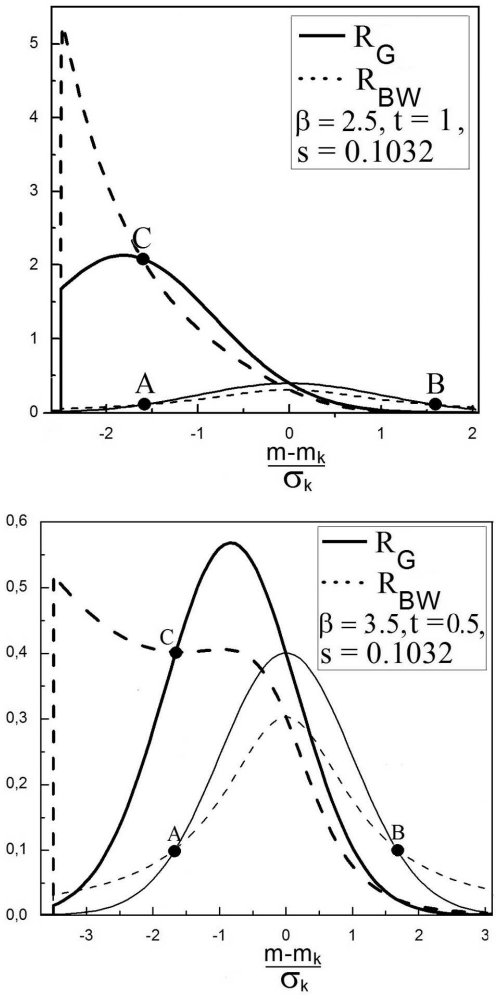

Fig. 10. Mass attenuations of the resonance enhancement factors R_G and $R_{\rm BW}$ are compared for two values of the reduced temperature $t = T/\sigma_k$. Upper (lower) panel corresponds to $t = 0.5$ ($t = 1$). The thin solid curve represents the Gaussian mass attenuation, while the thin dashed curve shows the Breit–Wigner one. The thick curves correspond to the integrands staying in Eqs. (26) (solid) and (27) (dashed). The intersection points A, B, and C are discussed in the text

and Gauss mass distributions used in Eqs. (26) and (27) get equal for $x_k^{\pm} \simeq \pm(1.6\pm0.1)$ depending on the value of β_k, where x denotes the dimensionless variable $\frac{m-m_k}{\sigma_k}$. These intersection points of two normalized distributions are denoted by points A and B in Fig. 10. Now it is clear that, if the threshold is located between $x = 0$ and $x = x_k^-$, i.e. for $-\beta_k \geq x_k^-$, then the enhancement factor of the Gaussian mass attenuation R_G is larger than $R_{\rm BW}$. A similar situation ex-

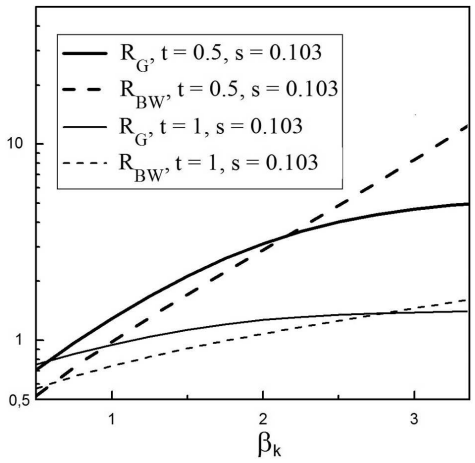

Fig. 11. β_k dependence of the resonance enhancement factor R is shown for two values of the reduced temperature $t = T/\sigma_k$. Thick (thin) curves correspond to $t = 0.5$ ($t = 1$). Solid curves represent the Gaussian mass attenuation of resonances, while the dashed curves show the results for the Breit–Wigner one

ists, if the threshold is not too below $x = x_k^-$, i.e., for $-\beta_k \lessapprox x_k^-$. However, if the threshold is located somewhat away from the intersection point $x = x_k^-$, i.e. for $-\beta_k \ll x_k^-$, then the Breit–Wigner mass attenuation is essentially enhanced near the threshold by the Boltzmann exponential, as one can see from the both panels of Fig. 10. Evidently, that effect gets stronger for lower values of temperature, and the dashed lines in Fig. 11 clearly demonstrate the exponential dependence for the Breit–Wigner enhancement factor $R_{\rm BW} \sim \exp[\beta_k/t_k]$ for $\beta_k > 2$.

It is of importance that the Breit–Wifner enhancement factor of the narrow and very narrow resonances is larger than the Gaussian one, if the threshold is located somewhat away from the mean resonance mass m_k. For example, at a temperature of 100 MeV for the $\omega(783)$-meson, which decays with a small width into three pions, these factors are $R_{\rm BW} \simeq 1.034$ and $R_G = 1$. We find a more dramatic difference at this temperature for the $\rho(770)$-meson, which decays into two pions: $R_{\rm BW} \simeq 1.79$ and $R_G \simeq 1.14$. Thus, for $-\beta_k \ll x_k^-$, which is the case for the $\omega(783)$-meson ($\beta_\omega \simeq 89.6$) and for the $\rho(770)$-meson ($\beta_\rho \simeq 7.54$), the Breit–Wigner enhancement factor $R_{\rm BW}$ exceeds the Gaussian one R_G, i.e. $R_{\rm BW} > R_G$.

It is also worth to note that, if the inequality $R_{\rm BW} < R_G$ takes place for a given resonance, then the Gaussian enhancement factor does not exceed usually 40 % of $R_{\rm BW}$, and it very seldom exceeds 50%, while we found many examples for $T < 100$ MeV that the opposite inequality for these enhancement factors can be, in fact, replaced by $R_{\rm BW} \gg R_G$. The typical examples of such a behavior are given by the thick curves in Fig. 11. The discussed properties of the enhancement factors allow one to naturally explain the fact that the chemical FO pressure within the HRGMBW can be twice larger than the one within the HRGMG (see an upper panel of Fig. 3), although the relative differences of the corresponding chemical FO temperatures and the baryonic chemical potentials are less than 6%. Thus, the presence of many resonances (even very narrow ones!), whose decay thresholds are far away from the peak of the resonance mass attenuation, i.e. for $-\beta_k \ll x_k^-$, leads to a strong enhancement of the HRGMBW pressure compared to the HRGMG pressure, while the latter is also enhanced compared to the HRGM0 pressure. For the energy density, such a conclusion is not obvious, since one has to take additionally the density of states with a given mass into account.

The first important result from this analysis is that there is no sense to discuss the mass spectrum of hadronic resonances, the empirical or Hagedorn one, without a treatment of their width. Clearly, the same is true for the QG bags which, according to the FWM [16, 17], are heavy wide resonances with mass M_B larger than $M_0 \simeq 2.5$ GeV and with the mean width of the form $\Gamma_B \simeq \Gamma_0(T) \left[\frac{M_B}{M_0}\right]^{1/2}$, where $\Gamma_0(T)$ is a monotonically increasing function of T and $\Gamma_0(T = 0) \in [400; 600]$ MeV. This range of the values of $\Gamma_0(T = 0)$ corresponds to the pseudocritical temperature $T_{\rm pc} \simeq 170 - 200$ MeV [16, 17] for the vanishing baryonic density. The value $\Gamma_0(T = 0) = 400$ MeV is well consistent with the results of the up-to-date lattice QCD thermodynamics [80, 81], but there is no guarantee that the lattice QCD data will not change in the future. Therefore below, we consider the whole range of values for the width $\Gamma_0(T)$ analyzed in [16, 17].

There are two interesting features of QG bags which are related to the above treatment. Thus, from the results of [16, 17] and from Eq. (19), one can find the temperature T_B^+ for the meson-like QG bags as

$$T_B^+ \simeq \frac{\Gamma_0^2(T)}{Q^2\, M_0\, (1 - \xi_B)} \simeq \frac{1}{(1 - \xi_B)} \times$$

$$\times \begin{cases} 11.5\text{–}26 \text{ MeV}, & \text{if } \Gamma_0(0) \simeq 0.4\text{–}0.6 \text{ GeV}, \\ 46\text{–}104 \text{ MeV}, & \text{if } \Gamma_0(90) \simeq 0.8\text{–}1.2 \text{ GeV}, \\ 140\text{–}315 \text{ MeV}, & \text{if } \Gamma_0(170) \simeq 1.4\text{–}2.1 \text{ GeV}, \end{cases} \quad (28)$$

where $\xi_B \equiv \frac{M_B^{\rm Th}}{M_B}$ denotes the ratio of the leading threshold mass $M_B^{\rm Th}$ of a bag to its mean mass M_B. In (28), the values of temperature T, which are given in the expression for $\Gamma_0(T)$, are measured in MeVs. Our justification to apply (28) to the meson-like QG bags at non-zero baryonic densities was given above.

Clearly, the range of ξ_B values can be between 0 and 1 for different bags. Therefore, according to above results, the bags with $\xi_B \to 1$ should have been essentially enhanced and sharpened, as the ordinary resonances. Moreover, according to (19), the meson-like QG bags should have had a small width $\Gamma_B^{\rm app} \simeq \frac{T\,T_B^+}{T_B^+ - T} \ln(2)$ in this case for $T \ll T_B^+$. Hence, such QG bags should have long life-time, or, in other words, there is a chance to observe such QG bags! We recall that the reason for why such bags are not observed in the experiments is naturally explained by the FWM [16, 17]: it is due to *the subthreshold suppression* (for more details, see a discussion after Eq. (42) in [17]).

On the other hand, Eq. (28) shows that the only hope to observe the QG bags exists, if $\xi_B \to 1$. Then, for chemical FO temperatures much below T_B^+, such bags could have a sufficiently long eigen lifetime of about $\tau_B \sim \frac{1}{\Gamma_B^{\rm app}} \simeq \frac{T_B^+ - T}{T\,T_B^+\,\ln(2)} \leq \frac{1}{T\,\ln(2)}$. Substituting $T \simeq 0.5\,T_{\rm H} \in [80; 90]$ MeV in the last inequality and using the estimate of Eq. (28) for $T = 90$ MeV with $\xi_B = 0.9$, one finds the most optimistic estimates for the QG bag eigen lifetime as $\tau_B \leq 3.3 \pm 0.3$ fm/c. On the other hand, for $\xi_B = 0.9$ and $T = 140$ MeV, one finds from (19) and (28) that $T_B^+ \simeq 1200$ MeV and $\Gamma_B^{\rm app} \simeq 100$–$120$ MeV. These estimates allow us to make the second important conclusion that *the appearance of sharp resonances (mesonic or/and baryonic) with the apparent width being in the interval between 50 to 120 MeV* at the chemical FO temperatures $T_{\rm QGB} \simeq 85$–140 MeV *that have the mass above 2.5 GeV and are absent in the tables of particle properties would be a clear signal of the QG bag formation.* Their possible appearance at the chemical FO as metastable states of finite systems created in relativistic nuclear collisions is justified by the FWM [16, 17]. At higher temperatures, such QG bags can be formed too, but their apparent width is larger, and their enhancement is less pronounced. The limiting values of ξ_B at T, for which the effect of resonance sharpening can exist, are determined by the relation $\Gamma_0^2(T)/T \geq Q^2\,M_0\,(1 - \xi_B)$. From the latter inequality, one can see that the condition $\xi_B \to 0.9$ can be relaxed, but, in this case, the temperature of the chemical FO gets higher.

In addition, one has to account for the statistical probability of the appearance of QG bags at a given temperature T. Relatively to a nucleon, the thermal probability of a QG bag of mass M_B is about $W = \left[\frac{M_B}{M_N}\right]^{1.5} \exp\left[\frac{(M_N - M_B)}{T}\right] R_B(T)$, where $M_N \simeq$ $\simeq 940$ MeV is the nucleon mass, and $R_B(T)$ is the resonance enhancement factor in a thermal medium. For $T = 140$ MeV and $M_B = M_0 \simeq 2.5$ GeV, one gets $W_B \simeq 3.85 \times 10^{-5} R_B$. It was shown above that, for such temperatures, the typical resonance apparent width values are about $\Gamma_B \simeq 100$–120 MeV, while the typical values of the resonance enhancement factor can be estimated as $R_B \simeq 10$–100 for $\beta_B \simeq 2.5$–4.5. Therefore, compared to a nucleon, the relative thermal probability of such QG bags is about $W_B \simeq 3.85 \times (10^{-4}$–$10^{-3})$, which is essentially larger than the relative probability of the J/ψ meson $W_{J/\psi} \simeq 1.19 \times 10^{-6}$ at the same temperature. Note that the chemical FO temperature $T \simeq 140$ MeV corresponds to the highest SPS energy of collision, at which the J/ψ mesons are safely measured. Therefore, these estimates give us a hope for that the decays of meson-like QG bags can, in principle, be measured in the energy range $\sqrt{s_{NN}} \simeq 4.3$–6 GeV.

5. Conclusions

Here, we developed the HRGM with the Gaussian mass attenuation of hadronic resonances. A successful fit of the particle yield ratios allowed us to elucidate an unprecedented jump of the number of effective degrees of freedom existing in the narrow energy range $\sqrt{s_{NN}} = 4.3$–4.9 GeV. It is remarkable that all realistic versions of the HRGM analyzed here demonstrate the same behavior. Therefore, the developed concept was named the non-smooth chemical FO. An effort to explain the non-smooth chemical FO led us to a conclusion that these irregularities can be related to the formation of QG bags at $\sqrt{s_{NN}} = 4.3$–4.9 GeV. Here, we give some arguments based of the FWM framework that the found irregularities, especially a jump

in the number of effective degrees of freedom, can serve as the signals of the QG bags formation.

We also analyzed the behavior of wide resonances in a thermal environment, calculated their apparent width for the Gaussian and Breit–Wigner mass attenuations, and found two new effects occurring, if the chemical FO temperature is small compared to the resonance width: *the near-threshold thermal resonance enhancement* and *the near-threshold resonance sharpening*. As was discussed, these effects formally appear due to the same reason, as the famous Gamow window for the thermonuclear reactions in stars. The found effects allowed us to naturally explain the fact that the HRGM, which accounts for the finite widths of hadronic resonances, generates higher pressure than the one with a zero resonance width. As an important application of the found effects, we studied the apparent width of the σ-meson for the Gaussian mass attenuation. The analysis showed that, for the temperatures below 92 MeV, the σ-meson can be rather narrow, and it has an apparent width of about or below 70 MeV. Thus, accounting for the σ-meson large width in a thermal medium allows us to justify, to some extent, the usage of the σ-like field theoretical models for the strongly interacting matter equation of state at temperatures below 92 MeV. It is clear that, at higher temperatures, the usage of the narrow σ-meson in field theoretical models cannot be justified within the HRGM, since it requires the microscopic approach.

The new effects are thoroughly compared for the Gaussian and Breit–Wigner mass attenuations, and it is shown that, under the same conditions, the Breit–Wigner width parametrization enhancement factor can be essentially larger than the Gaussian one, if the decay thresholds of a given resonance are far away from the resonance peak. Such a result helps one to understand the reason for why the chemical FO pressure of the HRGMBW can be twice larger than the one of the HRGMG, although the relative differences of the corresponding chemical FO temperatures and baryonic chemical potentials do not exceeds 6%. In the present work, a question of the correct parametrization of the resonance mass attenuation to be used for the phenomenological applications is addressed to the microscopic models, which do not provide us with the satisfactory prescriptions at the moment.

Finally, applying these new effects to the QG bags, we argue that the most optimistic chance to find the meson-like QG bags experimentally would be related to their sharpening and enhancement by a thermal medium. If this is the case, then the QG bags may appear directly or in decays as narrow resonances of apparent widths of about 50–120 MeV, which have the mass about or above 2.5 GeV and are absent in the tables of elementary particles.

The practical conclusions that can be drawn out of these findings can be important for planning the experiments at the FAIR (GSI) and at the Nuclotron (JINR) facilities. As we argued here, it is possible that the energy range associated with the onset of the quark-gluon-hadron mixed phase does not correspond to the Strangeness Horn energy $\sqrt{s_{NN}} \simeq 7.6$ GeV, but such an onset should be searched at the collision energies $\sqrt{s_{NN}} \simeq 4.3$–4.9 GeV.

The authors are thankful to A.B Larionov and I.N. Mishustin for valuable comments. K.A.B., A.I.I., and G.M.Z. acknowledge a support of the Fundamental Research State Fund of Ukraine, Project No. Ф58/175-2004. K.A.B. acknowledges a partial support provided by the Helmholtz International Center for FAIR within the framework of the LOEWE program launched by the State of Hesse.

1. A. Chodos *et. al.*, Phys. Rev. D **9**, 3471 (1974).
2. J.I. Kapusta, Phys. Rev. D **10**, 2444 (1981).
3. R. Hagedorn, Suppl. Nuovo Cimento **3**, 147 (1965).
4. R. Hagedorn and J. Ranft, Suppl. Nuovo Cimento **6**, 169 (1968).
5. C.J. Hamer and S.C. Frautschi, Phys. Rev. D **4**, 2125 (1971).
6. K.A. Bugaev, Phys. Rev. C **76**, 014903 (2007).
7. K.A. Bugaev, Phys. Atom. Nucl. **71**, 1615 (2008).
8. K.A. Bugaev, Phys. Part. Nucl. **38**, 447 (2007).
9. A.I. Ivanytskyi, Nucl. Phys. A **880**, 12 (2012).
10. K.A. Bugaev, V.K. Petrov, and G.M. Zinovjev, Phys. Part. Nucl. Lett. **9**, 397 (2012); and Phys. Atom. Nucl. **76**, 341 (2013).
11. A.I. Ivanytskyi, K.A. Bugaev, A.S. Sorin, and G.M. Zinovjev, Phys. Rev. E **86**, 061107 (2012).
12. I. Zakout, C. Greiner, and J. Schaffner-Bielich, Nucl. Phys. A **781**, 150 (2007) and references therein.
13. I. Zakout and C. Greiner, Phys. Rev. C **78**, 034916 (2008).
14. I. Zakout and C. Greiner, arXiv:1002.3119 [nucl-th].
15. L. Ferroni and V. Koch, Phys. Rev. C **79**, 034905 (2009).
16. K.A. Bugaev, V.K. Petrov, and G.M. Zinovjev, Europhys. Lett. **85**, 22002 (2009).

17. K.A. Bugaev, V.K. Petrov, and G.M. Zinovjev, Phys. Rev. C **79**, 054913 (2009).
18. D.B. Blaschke and K.A. Bugaev, Fizika B**13**, 491 (2004); Prog. Part. Nucl. Phys. **53**, 197 (2004); Phys. Part. Nucl. Lett. **2**, 305 (2005).
19. J. Cleymans and H. Satz, Z. Phys. C **57**, 135 (1993).
20. A. Andronic, P. Braun-Munzinger, and J. Stachel, Nucl. Phys. A **772**, 167 (2006) and references therein.
21. A. Andronic, P. Braun-Munzinger, and J. Stachel, Phys. Lett. B **673**, 142 (2009); ; Erratum-ibid. **678**, 516 (2009) and references therein.
22. D.R. Oliinychenko, K.A. Bugaev, and A.S. Sorin, Ukr. J. Phys. **58**, 211 (2013); Ukr. J. Phys. **58**, 939 (2013).
23. K.A. Bugaev, D.R. Oliinychenko, A.S. Sorin, and G.M. Zinovjev, Eur. Phys. J. A **49**, 30 (2013).
24. K.A. Bugaev *et al.,* Europhys. Lett. **104**, 22002 (2013).
25. J. Stachel, A. Andronic, P. Braun-Munzinger, and K. Redlich, arXive:1311.4662v1 [nucl-th].
26. C. Amsler *et al.*, Phys. Lett. B **667**, 1 (2008) [http://pdg.lbl.gov].
27. K.A. Bugaev and G.M. Zinovjev, Ukr. J. Phys. **55**, 586 (2010).
28. V.V. Sagun, A.I. Ivanytskyi, K.A. Bugaev, and I.N. Mishustin, Nucl. Phys. A **924**, 24 (2014).
29. W. Broniowski, W. Florkowski, and L.Y. Glozman, Phys. Rev. D **70**, 117503 (2004).
30. A. Andronic, P. Braun-Munzinger, and J. Stachel, Acta Phys. Polon. B **40**, 1005 (2009).
31. J. Cleymans and D. Worku, Mod. Phys. Lett. A **26**, 1197 (2011).
32. D. Hahn and H. Stöcker, Nucl. Phys. A **452**, 723 (1986).
33. K.G. Denisenko and St. Mrowczynski, Phys. Rev. C **35**, 1932 (1987).
34. M.I. Gorenstein, St. Mrowczynski, and D.H. Rischke, Phys. Lett. B **243**, 327 (1990).
35. J. Sollfrank, P. Koch, and U. Heinz, Z. Phys. C **52**, 593 (1991).
36. K.A. Bugaev, M.I. Gorenstein, and D.H. Rischke, Phys. Lett. B **255**, 18 (1991).
37. K.A. Bugaev, E.G. Nikonov, A.S. Sorin, and G.M. Zinovjev, JHEP **02**, 059 (2011); Ukr. J. Phys. **56**, 611 (2011).
38. S. Wheaton, J. Cleymans, and M. Hauer, Comput. Phys. Commun., **180**, 84 (2009).
39. W. Weinhold, B. Friman, and W. Nörenberg, Phys. Lett. B **433**, 236 (1998).
40. H. van Hees and R. Rapp, Phys. Lett. B **606**, 59 (2005).
41. M. Effenberger, E.L. Bratkovskaya, and U. Mosel, Phys. Rev. C **60**, 044614 (1999).
42. M. Effenberger and U. Mosel, Phys. Rev. C **60**, 051901 (1999); A.B. Larionov and U. Mosel, Phys. Rev. C **66**, 034902 (2002).
43. V.I. Kuksa, Phys. Part. Nucl. (in Russian) **45**, 998 (2014) and references therein.
44. J.L. Klay *et al.*, Phys. Rev. C **68**, 054905 (2003).
45. L. Ahle *et al.*, Phys. Lett. B **476**, 1 (2000); Phys. Lett. B **490**, 53 (2000).
46. B.B. Back *et al.*, Phys. Rev. Lett. **86**, 1970 (2001).
47. J.L. Klay *et al.*, Phys. Rev. Lett. **88**, 102301 (2002).
48. C. Pinkenburg *et al.*, Nucl. Phys. A **698**, 495c (2002).
49. P. Chung *et al.*, Phys. Rev. Lett. **91**, 202301 (2003).
50. S. Albergo *et al.*, Phys. Rev. Lett. **88**, 062301 (2002).
51. B.B. Back *et al.*, Phys. Rev. Lett. **87**, 242301 (2001).
52. B.B. Back *et al.*, Phys. Rev. C **69**, 054901 (2004).
53. S.V. Afanasiev *et al.*, Phys. Rev. C **66**, 054902 (2002).
54. S.V. Afanasiev *et al.*, Phys. Rev. C **69**, 024902 (2004).
55. T. Anticic *et al.*, Phys. Rev. Lett. **93**, 022302 (2004).
56. S.V. Afanasiev *et al.*, Phys. Lett. B **538**, 275 (2002).
57. C. Alt *et al.*, Phys. Rev. Lett. **94**, 192301 (2005).
58. S.V. Afanasiev *et al.*, Phys. Lett. B **491**, 59 (2000).
59. J. Adams *et al.*, Phys. Rev. Lett. **92**, 182301 (2004).
60. J. Adams *et al.*, Phys. Lett. B **567**, 167 (2003).
61. C. Adler *et al.*, Phys. Rev. C **65**, 041901(R) (2002).
62. J. Adams *et al.*, Phys. Rev. Lett. **92**, 112301 (2004).
63. J. Adams *et al.*, Phys. Lett. B **612**, 181 (2005).
64. A. Billmeier *et al.*, J. Phys. G **30**, S363 (2004).
65. K.A. Bugaev *et al.*, arXiv:1405.3575 [hep-ph] (accepted to Phys. Part. Nucl. Lett.).
66. M. Gazdzicki and M.I. Gorenstein, Acta Phys. Polon. B **30**, 2705 (1999).
67. see, e.g., J. Cleymans, H. Oeschler, K. Redlich, and S. Wheaton, Phys. Rev. C **73**, 034905 (2006).
68. V.V. Begun, M. Gazdzicki, and M.I. Gorenstein, Phys. Rev. C **88**, 024902 (2013).
69. V.V. Begun, M. Gazdzicki, and M.I. Gorenstein, Contribution 2.8 to the NICA White Paper, version 9.02, 7 of June, 2013. http://theor.jinr.ru/twiki/pub/NICA/NICAWhitePaper.
70. M. Gazdzicki, Z. Phys. C **66**, 659 (1995); J. Phys. G **23**, 1881 (1997).
71. M.I. Gorenstein, M. Gazdzicki, and K.A. Bugaev, Phys. Lett. B **567**, 175 (2003).
72. M. Gazdzicki, M. Gorenstein, and P. Seyboth, Acta Phys. Polon. B **42**, 307 (2011).
73. J. Engels, F. Karsch, J. Montway, and H. Satz, Nucl. Phys. B **205**, 545 (1982).
74. T. Celik, J. Engels, and H. Satz, Nucl. Phys. B **256**, 670 (1985).
75. M. Cheng et al., Phys. Rev. D **77**, 014511 (2008).
76. BNL-Bielefeld Collaboration, Phys. Rev. D **83**, 014504 (2011).
77. C.S. Rolfs and W.S. Rodney, *Cauldrons in the Cosmos* (Univ. of Chicago Press, Chicago, 1986).
78. C. Iliadis, *Nuclear Physics of Stars* (Wiley-VCH, Weinheim, 2007).
79. R. Garcia-Martin, J.R. Pelaez, and F.J. Yndurain, Phys. Rev. D **76**, 074034 (2007).
80. F. Karsch, Prog. Theor. Phys. Suppl. **168**, 237 (2007).

81. Y. Aoki *et al.*, Phys. Lett. B **643**, 46 (2006); Y. Aoki *et al.*, JHEP **06**, 088 (2009).

Received 29.08.14

К.О. Бугаєв, О.І. Іваницький,
Д.Р. Олійниченко, Е.Г. Ніконов,
В.В. Сагун, Г.М. Зінов'єв

НЕГЛАДКИЙ ХІМІЧНИЙ ФРІЗАУТ І ВИДИМА ШИРИНА ШИРОКИХ РЕЗОНАНСІВ ТА КВАРК-ГЛЮОННИХ МІШКІВ В ТЕРМОДИНАМІЧНОМУ СЕРЕДОВИЩІ

Р е з ю м е

В роботі розвинуто модель адронного резонансного газу з гаусовою шириною резонансів. Така модель дозволяє розглянути звичайні адрони та кварк-глюонні мішки єдиним чином і вивчити стійкість результатів, отриманих в різних формулюваннях моделі адронного резонансного газу. В цій роботі проведено успішний фіт 111 незалежних адронних множинностей, виміряних в зіткненнях ядер за енергій в системі центра мас $\sqrt{s_{NN}} = 2{,}7$–200 ГеВ. Також показано, що у вузькій області енергій зіткнення 4,3–4,9 ГеВ спостерігаються незвичайні нерегулярності у різних термодинамічних величин, знайдених за хімічного фрізаута. Найбільш визначною нерегулярністю є невідомий раніше стрибок числа ефективних степенів вільності в цьому вузькому інтервалі енергій, який спостерігається у всіх реалістичних версіях моделі адронного резонансного газу, включаючи модель із брейт–вігнерівською параметризацією ширини резонансів та модель із нульовою шириною всіх резонансів. Тому розвинута концепція названа негладким хімічним фрізаутом. Подано аргументи на користь того, що ці нерегулярності свідчать про можливе формування кварк-глюонних мішків. Для того, щоб розвинути інші можливі сигнали їх формування, нами вивчена видима ширина широких адронних резонансів та кварк-глюонних мішків. Обмірковано два нових ефекти, які генеруються для широких адронних резонансів та кварк-глюонних мішків термального середовища: біляпорогове термальне підсилення резонансів та біляпорогове термальне звуження резонансів. Також ці ефекти проаналізовано для брейт–вігнерівської параметризації ширини та показано, що, коли пороги розпадів резонансів знаходяться далеко від піка в розподілі маси резонансу, то така параметризація ширини веде до більшого підсилення тиску резонанса порівняно із гаусовою параметризацією ширини. На основі цих ефектів ми стверджуємо, що найбільш оптимістичний шанс експериментально знайти кварк-глюонні мішки пов'язаний з їхнім звуженням та підсиленням в термальному середовищі. В цьому випадку кварк-глюонні мішки можуть виникнути або в розпадах, як вузькі резонанси, які відсутні в таблицях елементарних частинок з шириною близько 50–120 МеВ і з масою близько або більше 2,5 ГеВ.